ELSEVIER

Chemical Engineering Science 60 (2005) 5759–5769

Chemical Engineering Science

www.elsevier.com/locate/ces

Photocatalytic reduction of selenium ions using different TiO_2 photocatalysts

Vi Nu Hoai Nguyen, Rose Amal*, Donia Beydoun

ARC Centre for Functional Nanomaterials, School of Chemical Engineering and Industrial Chemistry, University of New South Wales, Sydney, NSW 2052, Australia

Received 4 February 2005; received in revised form 29 March 2005; accepted 23 April 2005

Abstract

Comparative performance studies between different photocatalysts for reduction reactions are scarce. Here, Millennium PC500 and PC50 photoreactivities were investigated for selenite (Se(IV)) and selenate (Se(VI)) reduction to their elemental form (Se(0)) and compared with that of Degussa P25 TiO_2. Millennium PC500, with the highest surface area demonstrated the fastest photoreduction of Se(IV) and Se(VI), compared to P25 and Millennium PC50. Millennium PC50 and P25, which have comparable surface areas, showed similar photoreactivities. UV–Vis reflectance measurements and XRD characterisation revealed that the Se(0) deposits underwent phase transformation from amorphous to stable crystalline Se(0) during the drying and ageing process. Overall, the Millennium PCs appear to be promising photocatalysts for the photoreduction process.

Keywords: Environment; Multiphase reactions; Phase change; Photocatalytic reduction; Photochemistry; Titanium dioxide

1. Introduction

Titanium dioxide (TiO_2)-based photocatalysis is a technology of strategic and economic importance (Serpone et al., 1988). This method has the advantage of destroying organic pollutants and/or transforming inorganic ions into less toxic forms (Chen and Ray, 2001; Howe, 1998; Litter, 1999). Furthermore, as photocatalysis can reduce metals to their elemental form, the metals can be readily recovered (Litter, 1999).

The photocatalytic process involves the activation of a semiconductor catalyst with light. This produces photoexcited electrons and holes that can participate in different redox reactions. Among various semiconductor oxides commonly used in photocatalysis, TiO_2 in both anatase and rutile forms has been found the most suited for the degradation of various environmental contaminants, including organic and inorganic compounds.

Of the two crystalline forms, anatase has typically shown a better photocatalytic activity than rutile (Sclafani et al., 1990a; Sclafani and Herrmann, 1996). This has been attributed to the slower charge carrier recombination rates of anatase and its more negative conduction band position. In addition, for some reactions the O_2 adsorbed on the TiO_2 surface is important as an electron acceptor and can affect the activity. O_2 adsorption depends on the surface properties of the catalyst such as degree of hydroxylation and surface area (Arabatzis et al., 2002; Campostrini et al., 1994). These are typically lower for rutile TiO_2, which is often prepared at high temperatures.

While Degussa P25 TiO_2 has in the past been considered the benchmark photocatalyst, more recently various new TiO_2 photocatalysts have been produced at a commercial scale and their photocatalytic activities are being gradually assessed. New commercially available photocatalysts that have been mentioned in the literature include Millennium PCs and Hombikat UV100 (Arslan et al., 2000; Herrmann et al., 2002; Hufschmidt et al., 2002; Wang et al., 2002, 2004),

* Corresponding author. Tel.: +61 2 9385 4361; fax: +61 2 9385 5966.
E-mail address: r.amal@unsw.edu.au (R. Amal).

0009-2509/$ - see front matter © 2005 Elsevier Ltd. All rights reserved.
doi:10.1016/j.ces.2005.04.085

Tioxides (Sclafani et al., 1990a,b; Sclafani and Herrmann, 1996) and Ishihara ST-01 (Almquist and Biswas, 2002).

Degussa P25 was found to perform better than Hombikat UV100 for the mineralisation of phenol (Tahiri et al., 1996) and 4-chlorophenol (Theuric et al., 1996). Interestingly, Hombikat UV100 outperformed Degussa for the photooxidation of methanol at a catalyst loading of more than $2.5\,g\,l^{-1}$ and vice versa below $2.5\,g\,l^{-1}$ (Wang et al., 2002). Studying the photoreduction of Hg(II), Wang et al. (2004) have also found that Hombikat UV100 performed better than Degussa P25 at a loading of greater than $2\,g\,l^{-1}$. These differences were attributed to the light absorption properties of the two catalysts. Hombikat UV100 was also found to perform better than Degussa P25 for the simultaneous photoreduction of Cr(VI) and photooxidation of salicylic acid (Colon et al., 2001).

When comparing Degussa P25 and Millennium PC500 for the photodegradation of simulated dyehouse effluents, Arslan et al. (2000) observed no clear correlation between initial dark adsorption of the reactants and the photonic efficiency, suggesting that not only the catalyst but also the physical–chemical properties of the degraded compounds affected the removal efficiency. However, Guillard et al. (2003) observed a correlation between higher dark adsorption of different dyes on PC500 compared to P25 and better photoreactivities, indicating that these photocatalytic reactions essentially occurred in the adsorbed phase at the surface of TiO_2. A better performance of the Millennium PCs (PC10, PC25 and PC50) compared to Degussa P25 TiO_2 was also found for the photodegradation of 4-chlorophenol (Herrmann et al., 2002).

The above studies show that photocatalytic reactions are inherently complex and involve many parameters, a number of which originate with the chosen photocatalyst. While most of these studies have focused on the degradation of organic compounds, little information is available to guide the selection of a photocatalyst for photocatalytic reduction reactions for which different issues and considerations may arise. In this report, the photocatalytic reduction of selenium ions (selenite (Se(IV)) and selenate (Se(VI))) was studied using TiO_2 Millennium PC samples (PC500 and PC50) as photocatalysts. The results were compared to those obtained using TiO_2 Degussa P25.

Selenium was chosen in this study, as it is one of the elements of environmental concern on which we have carried out a number of studies (Nguyen et al., 2004; Tan et al., 2002, 2003). The pollution of selenium is largely due to its release from waste materials from mining, agricultural, petrochemical and industrial manufacturing operations (Lemly, 2004). In the environment, selenium commonly exists in four different oxidation states: selenide ($Se(2^-)$), elemental selenium (Se(0)), selenite (Se(IV)) and selenate (Se(VI)). Depending on pH of the solution, these species can be present as Se^{2-}, SeO_3^{2-} and SeO_4^{2}, and their protonated anions as HSe^-, $HSeO_3^-$ and $HSeO_4^-$, respectively (Seby et al., 2001).

2. Experimental

2.1. Chemicals

TiO_2 Degussa P25 and Millennium PC500 and PC50 were used as photocatalysts. Sodium selenite, sodium selenate, formic acid, perchloric acid and sodium hydroxide were all of reagent grade and used without further purification. Water used was Milli-Q deionised water.

2.2. Apparatus

Photocatalytic experiments were performed in a glass reactor. This has been described in greater detail elsewhere (Tan et al., 2002). It had a lid equipped with sample ports, which could be sealed. Oxygen was evacuated from the system by purging with nitrogen. The contents of the reactor were stirred throughout the experiment. For each experiment, a 1000 ml reaction solution was employed and illuminated by a 200 W Hg lamp, providing UV light of wavelength below 380 nm with the main emission peak at 253.7 nm. The pH of the solution was controlled manually with $HClO_4$ and NaOH to maintain pH 3.5 for the photocatalytic reduction of selenium ions. As the reduction of Se(IV) and Se(VI) could result in the production of toxic H_2Se gas, the reactor system was connected to two scrubbers in series, containing $CuSO_4$ and NaOH to capture the H_2Se gas.

2.3. Procedure

Our previous studies found that in the presence of P25 as the photocatalyst and formic acid as a hole scavenger, at pH 3.5, Se(IV) and Se(VI) could be photoreduced to the elemental form (Se(0)) according to the overall reactions (1) and (2), respectively (Nguyen et al., 2004; Tan et al., 2003).

$$HSeO_3^- + 2HCOO^- + 3H^+ \xrightarrow{h\nu,TiO_2} Se^0 + 3H_2O + 2CO_2, \quad (1)$$

$$SeO_4^{2-} + 3HCOO^- + 5H^+ \xrightarrow{h\nu,TiO_2} Se^0 + 4H_2O + 3CO_2. \quad (2)$$

The identified optimum conditions of $300\,mg\,C\,l^{-1}$ of formic acid and reaction pH of 3.5 were used in this study. Prior to irradiation, a solution containing selenium ions (either as sodium selenite or sodium selenate), formic acid and the TiO_2 photocatalyst (at a loading of $1.5\,g\,l^{-1}$) were allowed to equilibrate for 20 min (these will be referred to in the text as the dark adsorption experiments). An aliquot of this suspension was collected and immediately filtered through a 0.22 μm membrane filter. The filtrate was then analysed for selenium and total organic carbon (TOC). This concentration was taken as the initial concentration in solution at the beginning of the photoreduction reaction. Dark adsorption was taken as the difference between the concentration of selenium added to the system and the concentration of selenium

at the beginning of the photoreduction reaction. At the end of the dark adsorption period, the Hg lamp was switched on. The photoreaction period was determined according to the initial Se precursor and concentration. Aliquots were taken at time intervals and then used to measure the selenium and TOC remaining in solution.

2.4. Analysis

A Perkin-Elmer Optima 3000 ICP-OES spectrometer was used for the Se analysis. TOC analysis ($mg\,C\,l^{-1}$) was obtained using Shimadzu TOC-V CSH analyser. Each sample was analysed in triplicate. All analyses were obtained with a relative standard deviation (RSD) of less than 3% for the selenium measurements and less than 2% for the TOC measurements.

The photon flux in the reaction system was found to be 3.08×10^{-6} einstein $l^{-1}\,s^{-1}$ using ferrioxalate actinometry (Calvert and Pitts, 1966; Hatchard and Parker, 1956).

2.5. Characterisation studies

The Brunauer–Emmett–Teller (BET) surface area was determined using a Micromeritics ASAP 2000 BET surface analyser. Zeta potentials and dispersed particle size were determined using ZetaPALS from Brookhaven Instrument Co. High resolution transmission electron microscopy (HRTEM) images were obtained using a Philips CM200. Samples for electron microscopy were prepared by suspending small amounts of the photocatalysts in ethanol in an ultrasonic bath and three droplets of the suspensions were placed in carbon-coated copper grids.

UV–Vis diffuse reflectance was carried out using Varian Carry 5 UV–Vis–NIR spectrometer and employing $BaSO_4$ as reference. The resulting diffuse reflectance spectra were then related to absorption and scattering parameters using Kubelka–Munk remission function (Eq. (3.3)) (Delgass et al., 1979)

$$F(R_\infty) = \frac{K}{S} = \frac{(1 - R_\infty)^2}{2R_\infty}, \tag{3}$$

where R is the diffuse reflectance, and K and S are absorption and scattering coefficients, respectively.

Thermogravimetric analysis (TGA) was conducted using a Hi-Res Modulated TGA 2950 Thermogravimetric Analyzer (TA instrument). The crystalline phases of samples were determined by powder X-ray diffraction (XRD), using a Siemens Diffractometer D5000 with CuKα radiation.

3. Results and discussion

3.1. Characteristics of TiO_2 materials

Degussa P25 and Millennium PC photocatalysts are produced by different routes. P25, which generally contains 99.5% pure TiO_2, is produced in a high-temperature (greater than 1200 °C) process by flame hydrolysis of $TiCl_4$ in the presence of hydrogen and oxygen (Mills and Le Hunte, 1997). PC500 and PC50 on the other hand are produced by the sol–gel method. Table 1 shows some of the physical properties of the Degussa and Millennium photocatalysts.

PC500 and PC50 contain mainly anatase while P25 consists of 80% anatase and 20% rutile. PC500 has the smallest crystallite size and a surface area almost sixfold that of PC50 and P25. When comparing the dispersive particle size, all the particles were found to be aggregated with PC500 and PC50 being more compact compared to P25. This was also observed under the TEM as shown in Fig. 1. P25 and the PCs had similar zeta potentials at pH 3.5 even though they were prepared by different methods.

Fig. 2 shows the absorbance spectra of P25, PC500 and PC50. These spectra were derived from diffusion reflectance measurements using the Kubelka–Munk relationship. The absorbance spectrum obtained for Degussa P25 TiO_2 had an absorbance onset at around 380 nm with no absorption in the visible range. Compared to P25, PC500 and PC50 had a sharper absorbance edge, which was slightly blue shifted. This could be due to the fact that PC500 and PC50 have a smaller crystallite size compared to P25 and that the PCs contain only anatase TiO_2 while P25 consists of both anatase and rutile. It should be noted that the absorbance onset indicates the bandgap energy of the semiconductor, which

Table 1
Physical characteristics of TiO_2 catalysts

Catalyst	P25	PC500	PC50
Surface area ($m^2\,g^{-1}$) BET	48	374	53
Particle size (crystallites) (nm)	30[a]	10–15[b]	20–30[b]
Pore size (Å)	104	54	219
Composition	80% anatase, 20% rutile[a]	> 99.5% anatase[b]	> 99% anatase[b]
Dispersive particle size (nm)	200–215	600–700	700–800
Zeta potential at pH 3.5 (mV)	+9.1	+10.8	+8.8

[a]Adopted from Mills and Le Hunte, 1997.
[b]Provided by the particle manufacturer.

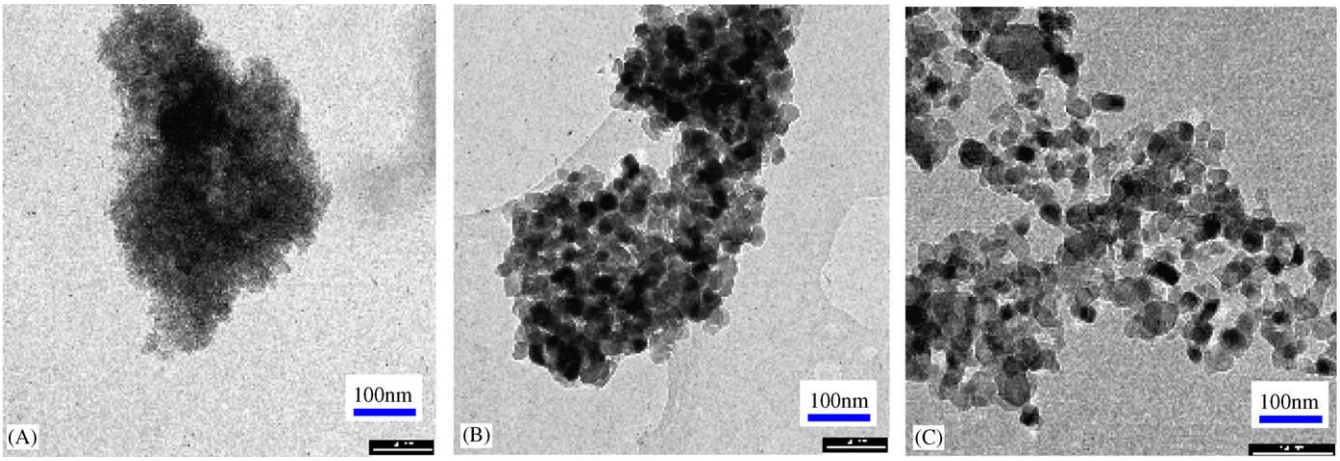

Fig. 1. TEM images the different TiO_2 photocatalyst powders in suspension (A) PC500; (B) PC50; and (C) P25.

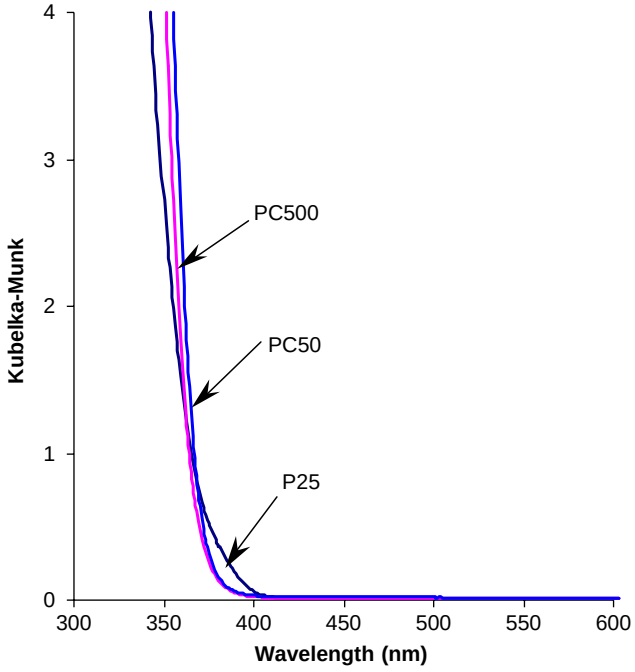

Fig. 2. Absorbance spectra of TiO_2 materials of interest.

should not be different whether the particles are present as dry solid or suspended in an aqueous medium.

3.2. Effect of different photocatalysts on dark adsorption of selenium ions

Our previous study (Tan et al., 2002) found that using P25 as the photocatalyst for 15 min was sufficient for Se(IV) and Se(VI) to reach adsorption equilibrium. Hence, in this study, dark adsorption experiments were carried out for 20 min to ensure that the equilibrium was obtained. The results of the dark adsorption studies are shown in Table 2 in which PC500 demonstrated much greater adsorption for selenate and selenite ions than P25 and PC50. P25 and PC50 adsorbed a similar amount of Se(IV) and Se(VI) ions. As was noted earlier, all three photocatalysts had a comparable surface charge at pH 3.5. Based on this, it is concluded that the greater adsorption of PC500 is due to its higher surface area, while the comparable adsorption of PC50 and P25 is due to their similar surface areas. A greater adsorption of Se(IV), compared to that of Se(VI), was obtained for all three TiO_2 materials. This can be attributed to the different chemical structures of the two ions, which affects the nature of the bonds formed during the sorption process (Cotton and Wilkinson, 1988; Sharmasarkar and Vance, 2002).

Table 2
Adsorption of selenium at pH 3.5

Catalysts	P25	PC500	PC50
Set 1: Se (IV) 20 mg l^{-1} [a]			
Adsorption (*mg* g^{-1} *catalyst*)	6.9 (±0.4)	12.9 (±0.8)	—
Set 2: Se (IV) 40 mg l^{-1} [a]			
Adsorption (*mg* g^{-1} *catalyst*)	8.3 (±0.5)	23.9 (±1.4)	7.3 (±0.4)
Set 3: Se (VI) 20 mg l^{-1} [a]			
Adsorption (*mg* g^{-1} *catalyst*)	2.5 (±0.2)	6.4 (±0.4)	—
Set 4: Se (VI) 40 mg l^{-1} [a]			
Adsorption (*mg* g^{-1} *catalyst*)	4.5 (±0.3)	11.9 (±0.7)	3.9 (±0.2)

[a] Initial concentrations of selenium ions.

3.3. Effects of different photocatalysts on photoreduction of selenium ions

In the following, photocatalytic activities of the catalysts of interest were tested and compared to examine the implications of particle properties and preparation methods. The results are presented in Figs. 3 and 4.

From Figs. 3 and 4, it can be seen that for all cases, PC500 showed better performance than P25 and PC50 for Se(IV) and Se(VI) photoreduction. In order for selenium

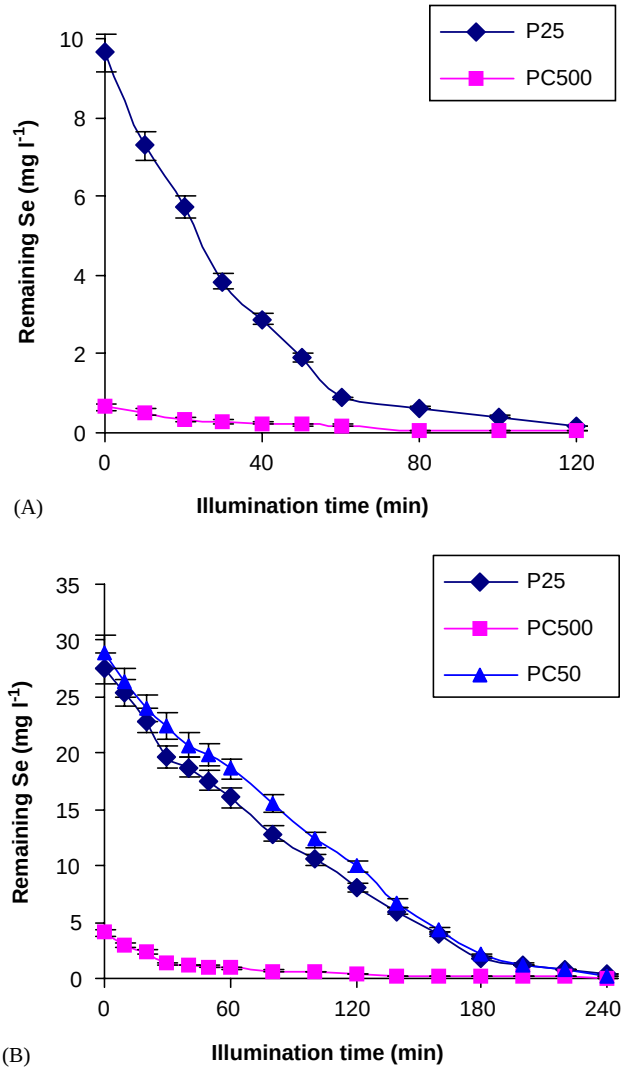

Fig. 3. Photocatalytic reduction of selenite (Se(IV)) using P25, PC500 and PC50 as catalysts. Conditions: catalyst loading: 1.5 g l^{-1}; dark adsorption: 20 min; hole scavenger: 300 mg C l^{-1} of formic acid; pH: 3.5; N_2 purging; initial Se(IV) concentrations: (A) 20 mg l^{-1}; (B) 40 mg l^{-1}.

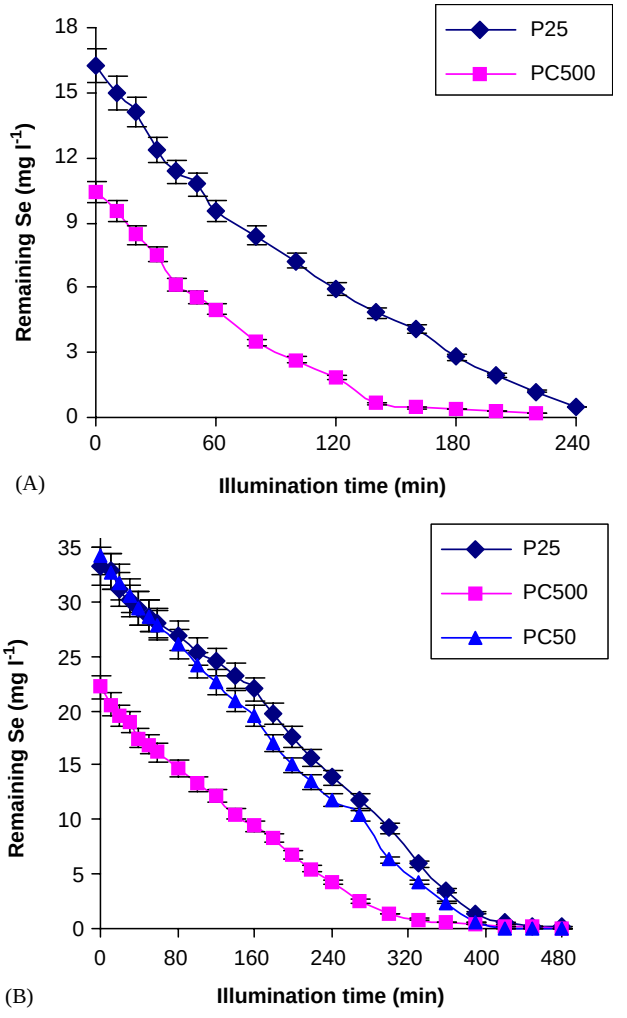

Fig. 4. Photocatalytic reduction of selenate (Se(VI)) using P25, PC500 and PC50 as catalysts. Conditions: catalyst loading: 1.5 g l^{-1}; dark adsorption: 20 min; hole scavenger: 300 mg C l^{-1} of formic acid; pH: 3.5; N_2 purging; initial Se(VI) concentrations: (A) 20 mg l^{-1}; (B) 40 mg l^{-1}.

ions to be photoreduced, they must first be adsorbed on the surface of the photocatalyst (Sanuki et al., 1999), hence the greater adsorption capacity of PC500 for selenium ions is believed to have led to the improved performance of this catalyst. The correlation between higher photoreduction rates and enhanced adsorption can be observed when comparing the photoreduction of Se(IV) with Se(VI). For all the TiO_2 materials used, the photoreduction of Se(IV) proceeded much faster than that of Se(VI). Starting with the same initial concentration, 20 mg l^{-1} of Se(IV) needed 2 h for its complete removal from solution while 4 h were needed to remove 20 mg l^{-1} Se(VI). Similarly, it took 8 h to remove 40 mg l^{-1} of Se(VI) while only 4 h were needed to remove 40 mg l^{-1} Se(IV). This is also attributed to the fact that to reduce Se(IV) to Se(0), only 4 electrons are needed while 6 electrons are required to reduce Se(VI) as has been discussed in our previous study (Nguyen et al., 2004). P25 and PC50, whose adsorption capacities were comparable, also displayed similar photocatalytic activities for the reduction of Se(IV) and Se(VI).

On the other hand, it is noted from Fig. 4 that although the adsorption of Se(VI) on PC500 was much greater than that on P25, the initial photoreduction rate of Se(VI) in the presence of PC500 was not much different from that in the presence of P25. To confirm whether in fact the removal of Se ions was due to photocatalytic reduction rather than adsorption, after 140 min of illuminating the solution, the light was turned off, the particles were recovered and re-suspended in 0.1 mM NaOH solution for 2 h. This was to desorb any Se(VI) that had not been reduced by the photocatalytic reduction process. This analysis was carried out for experiments with P25 and PC500 using Se(VI) concentration of 20 mg l^{-1} in the presence of 300 mg C l^{-1} of formic acid.

Table 3
Photocatalytic reduction activities of TiO_2 materials of interest

Catalysts	P25	PC-500
Se(VI) 20 mg		
Se(VI) remaining in solution after 140 min illumination (mg)	6.10 (±0.30)	0.86 (±0.05)
Se(VI) adsorbed on catalyst after 140 min illumination (mg)	0.20 (±0.01)	0.10 (±0.01)
Se(VI) deposited on catalyst surface (mg)	13.7 (±1.4)	19.0 (±1.4)

The results (presented in Table 3) show that with an initial Se(VI) amount of 20 mg after 140 min of illumination 0.86 mg of selenium remained in the solution when using the PC500 photocatalyst, compared to 6.1 mg when P25 was used. When the particles were collected and washed with NaOH, only 0.1 and 0.2 mg of Se ions were desorbed from the surface of PC500 and P25, respectively. This indicates that the removal of Se ions from the solution under illumination was due to the photocatalytic reduction process which converted the Se ions to Se(0) deposits. It can also be seen from the mass balance that after 140 min of illumination up to 19 mg of selenium was photoreduced using PC500, compared to only 13.7 mg when P25 was used. This indicates that PC500 was more effective in photoreducing selenium ions to their elemental form than P25.

3.4. Optimisation of formic acid hole scavenger concentrations for the photoreduction of selenium ions in the presence of PC50 and PC500

The photoreduction of Se(VI) in the presence of formic acid has been shown to involve a competitive adsorption process (Tan et al., 2002, 2003). Given that PC500 has a higher surface area and different adsorption properties to P25, it was of value to investigate the effect of formic acid concentrations on selenium photoreduction using PC500 and PC50 as photocatalysts.

The results for the photocatalytic reduction experiments in the presence of different formic acid concentrations using PC500 and PC50 are presented in Figs. 5, 6 and 7, respectively. The concentrations of selenium ions at time 0 were the difference between the initial and the remaining selenium concentrations in solution after the dark adsorption period. As can be seen from these figures, an increase in the formic acid concentration from 25 to 600 mg C l^{-1} led to a slight decrease in the dark adsorption of Se(IV) and Se(VI). This could be due to the fact that a higher concentration of formic acid had resulted in a greater amount of formate ions available to be adsorbed on the surface of the catalysts, leaving fewer adsorption sites for selenium ions to adsorb.

Despite the highest adsorption of selenium ions in the presence of 25 mg C l^{-1} of formic acid, the faster photoreduction rates of selenium ions were observed in the presence of formic acid $\geqslant$100 mg C l^{-1}. In addition, the lower formic acid concentrations of 25 mg C l^{-1} (Figs. 5 and 6) and 50 mg C l^{-1} (Fig. 7) resulted in incomplete removal of Se(IV) and Se(VI) for the allowed illumination periods. We have previously shown that the adsorption of both formic acid and selenium ions on the surface of the P25 TiO_2 photocatalyst is important for the photoreduction of selenium ions (Tan et al., 2003). This was further explored in the following studies on the adsorption of formic acid on the PC photocatalysts. The results are shown in Table 4.

It can be seen from Table 4 that as the initial Se ions concentration increased from 20 to 40 mg l^{-1}, the amount of selenium adsorbed on the surface of the PC500 photocatalyst also increased; however, with an initial concentration of 100 mg C l^{-1} the adsorption of formic acid remained mostly unchanged. This was true for both the Se(IV) and Se(VI) ions and also when PC50 was used as the photocatalyst. Furthermore, even though PC500 has a surface area sixfold that of PC50, the two photocatalysts had comparable

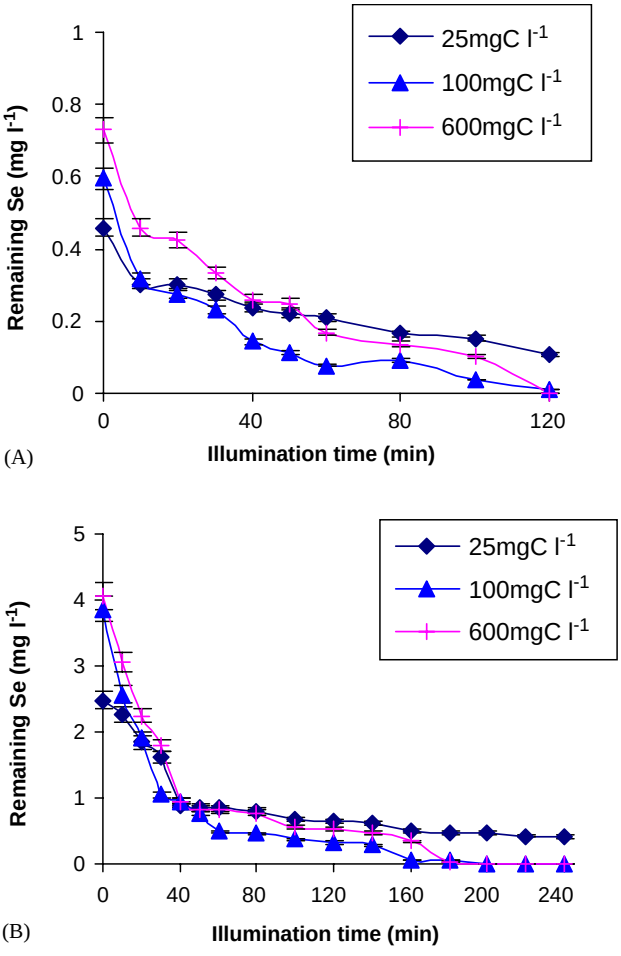

Fig. 5. Photoreduction of Se(IV): (A) 20 mg l^{-1}; (B) 40 mg l^{-1} using PC500 in the presence of various formic acid concentrations (25, 100, and 600 mg C l^{-1}). Conditions: catalyst loading: 1.5 g l^{-1}; dark adsorption: 20 min; pH: 3.5; N_2 purging.

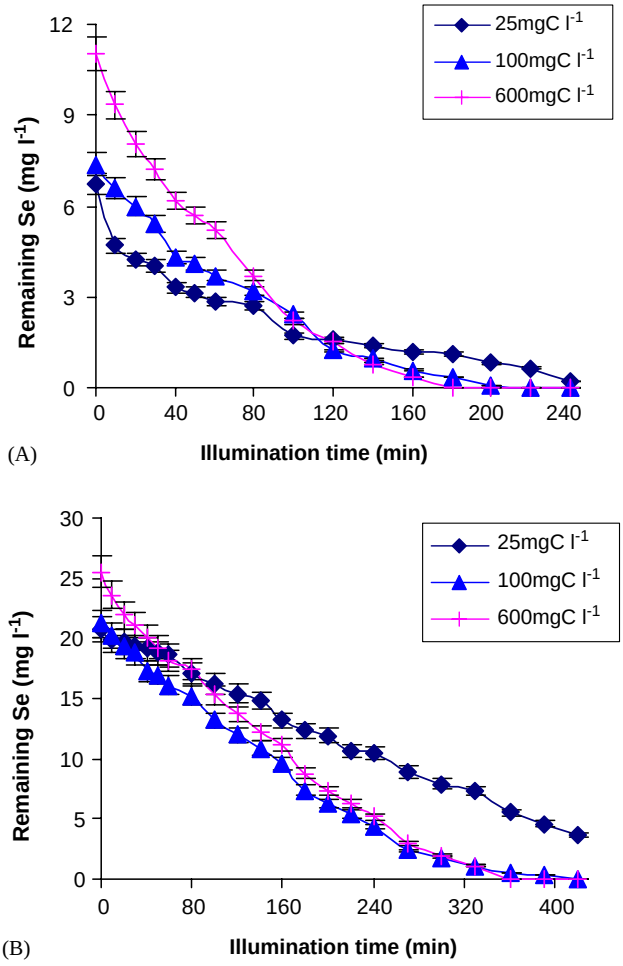

Fig. 6. Photoreduction of Se(VI): (A) 20 mg l^{-1}; (B) 40 mg l^{-1} using PC500 in the presence of various formic acid concentrations (25, 100, and 600 mg C l^{-1}). Conditions: catalyst loading: 1.5 g l^{-1}; dark adsorption: 20 min; pH: 3.5; N_2 purging.

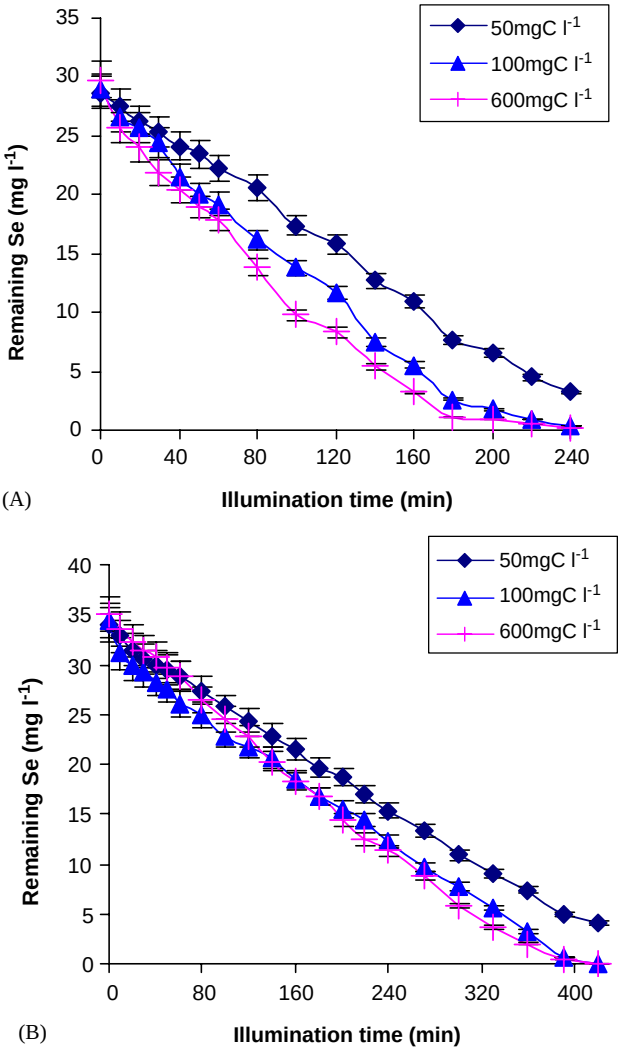

Fig. 7. Photoreduction of 40 mg l^{-1}: (A) Se(IV); (B) Se(VI) using PC50 in the presence of various formic acid concentrations (50, 100, and 600 mg C l^{-1}). Conditions: catalyst loading: 1.5 g l^{-1}; dark adsorption: 20 min; pH: 3.5; N_2 purging.

adsorption of formic acid. This shows that under the reaction conditions, only a limited amount of formic acid could be adsorbed on the surface of the catalyst. This could become a limiting factor for the photoreduction of selenium ions as both formic acid and selenium ions need to be adsorbed on the surface of the TiO_2. Hence, the decrease in the overall removal of selenium ions at formic concentrations lower than 100 mg C l^{-1} (Figs. 5–7) is postulated to be due to insufficient formic acid in the system.

3.5. Characterisation of the resulting powders

During the photocatalytic reduction of Se(IV) and Se(VI) using P25, PC500 and PC50 as the photocatalysts, the white colour of TiO_2 changed to orange-pink as Se(0) was deposited. Samples for the UV–Vis reflectance measurements

Table 4
Adsorption of formic acid (100 mg C l^{-1})

Precursor/concentration (mg l^{-1})	mg C formic g^{-1} catalyst		mg Se g^{-1} catalyst	
	PC500	PC50	PC500	PC50
Se(IV)20	7.93 (±0.48)		12.9 (±0.9)	
Se(IV)40	6.93 (±0.42)	6.60 (±0.40)	24.1 (±1.7)	7.4 (±0.5)
Se(VI)20	7.85 (±0.47)		8.4 (±0.6)	
Se(VI)40	7.13 (±0.43)	6.56 (±0.40)	12.5 (±0.9)	3.7 (±0.2)

were collected by filtration and the wet filtered powders retained the orange-pink colour. After the Se-P25 and Se-PC50 powders were dried in an oven overnight at 60 °C their colour changed to purple and grey, respectively, while the Se-PC500 particles remained orange pink. The colour of Se-PC500 did, however, change to grey after 2 weeks of ageing at room temperature.

The absorbance spectra from the UV–Vis reflectance analysis of the dried Se-PC500 (orange-pink), aged-dried Se-PC500 (grey) and the dried Se-PC50 (grey) are shown in Figs. 8A, 8B and 9, respectively. The optical properties of Se-P25 particles (purple) were investigated in our earlier publication (Nguyen et al., 2004) and typical absorbance spectra of this system were included in Figs. 8A, 8B and 9 for comparison. The absorbance spectra were obtained from the reflectance measurements using the Kubelka–Munk relationship.

In Figs. 8 and 9, the absorption spectra of the dried Se-PC500 particles (Fig. 8A), aged-dried Se-PC500 particles (Fig. 8B) and dried Se-PC50 (Fig. 9) can be divided into three regions: < 400, 400–580 and 580–730 nm. The region below 400 nm with an absorbance onset at around 380 nm can be assigned to the TiO_2 particles. A difference in the spectra between the dried Se-PC500, the aged-dried Se-PC500 and the dried Se-PC50 was observed in the regions 400–580 and 580–730 nm. The absorbance spectrum of the dried Se-PC500 (Fig. 8A) showed a steep absorbance increase from 580 to 400 nm, while in the same region, the aged-dried Se-PC500 (Fig. 8B) had a constant absorbance. The dried Se-PC50 had a small hump at around 450 nm (inset, Fig. 9). Additionally, the aged-dried Se-PC500 (Fig. 8B) and the dried Se-PC50 (Fig. 9) showed a sharp absorbance onset around 680 nm with a strong absorbance within the region of 580–730 nm, while the dried Se-PC500 (Fig. 8A) sample had weak absorbance in this 580–730 nm region.

Red amorphous Se does not have a sharp absorption edge (Mandough, 1993). Its activation has been approximated to be between 1.9 (650 nm) and 2.1 eV (580 nm) (Al-Ani et al., 1990; Mandough, 1993; Peled and Perakh, 1985). In addition, on studying the optical absorption of a red Se(0) solution, Rajalakshmi and Arora, 1999 found that the red Se solution had an absorbance onset at 2.69 eV (460 nm). Hence, the absorbance of the dried Se-PC500 starting at 580 nm can be attributed to the presence of amorphous Se. In addition, the small hump at around 450 nm in the absorbance of the dried Se-PC50 (Fig. 9, inset) may also be suggestive of the presence of a small fraction of amorphous Se.

On examining the absorbance spectra obtained for the Se–TiO_2 powders recovered from the photoreduction of selenium ions using the P25 photocatalyst (sample e in Figs. 8A, 8B and 9), an absorbance onset at around 680 nm (1.82 eV) and a hump at around 450 nm were observed. In our previous study on these Se–TiO_2 systems, these peaks were assigned to absorption by Se(0) deposits (Nguyen et al., 2004). It is known that elemental selenium has different allotropes (red monoclinic, red amorphous, grey "metallic" hexagonal and

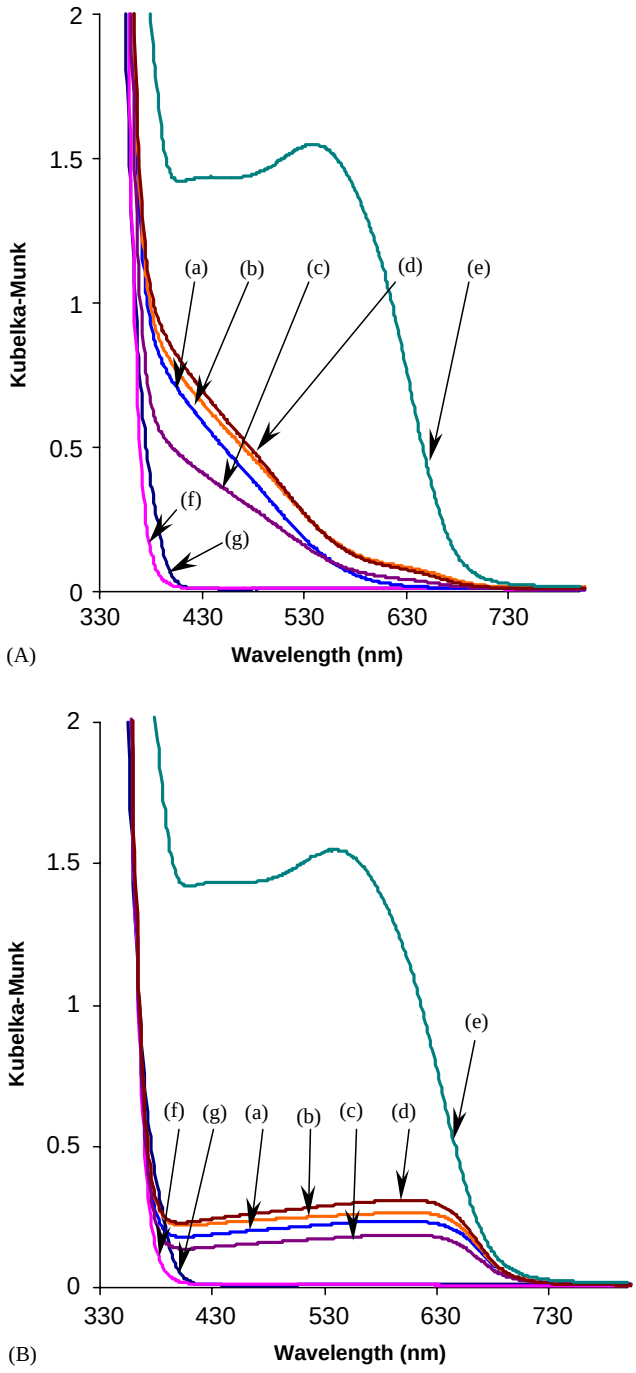

Fig. 8. Absorbance spectra of (A) dried PC500; (B) aged-dried PC500 obtained after selenium ion photoreduction. (a) Initial Se(IV) = 20 mg l^{-1}; (b) initial Se(IV) = 40 mg l^{-1}; (c) initial Se(VI) = 20 mg l^{-1}; (d) initial Se(VI) = 40 mg l^{-1}; Samples (e,f) are included for comparison on both graphs, (e) P25 after photoreduction of 20 mg l^{-1} Se(IV); (f) pure PC500 and (g) pure P25.

black Se) and that the amorphous Se can be transformed to the stable grey form with the heat energy of 5–10 kJ mol^{-1} of Se atoms (Greenwood and Earnshaw, 1997). In addition, on studying the ageing of amorphous Se, Mandough (1993) found that the energy gap for amorphous Se (2.05 eV) was shifted to 1.65 eV for metallic Se. Furthermore, it has been

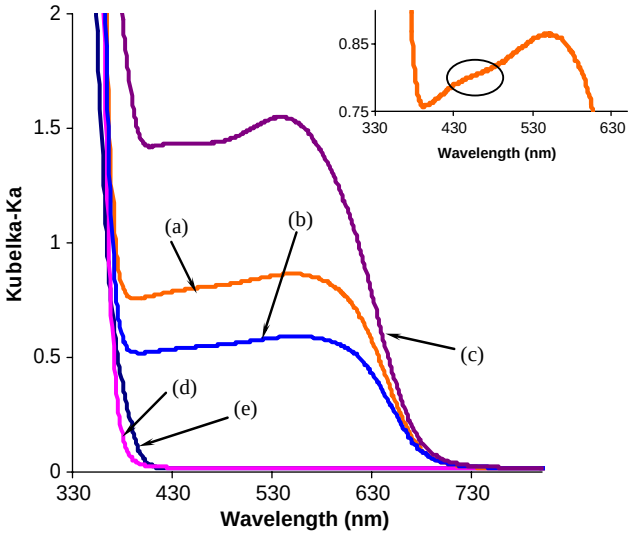

Fig. 9. Absorbance spectra of dried PC50 obtained after photoreduction of selenium ions. (a) Initial Se(IV) = 40 mg l^{-1} and (b) initial Se(VI) = 40 mg l^{-1}; Samples (c–e) are included for comparison; (c) P25 after photoreduction of 20 mg l^{-1} Se(IV); (d) pure PC50; (e) pure P25. Inset: sample (a) with an expanded *y*-axis, showing the hump at around 450 nm. A similar hump was also observed for sample (b).

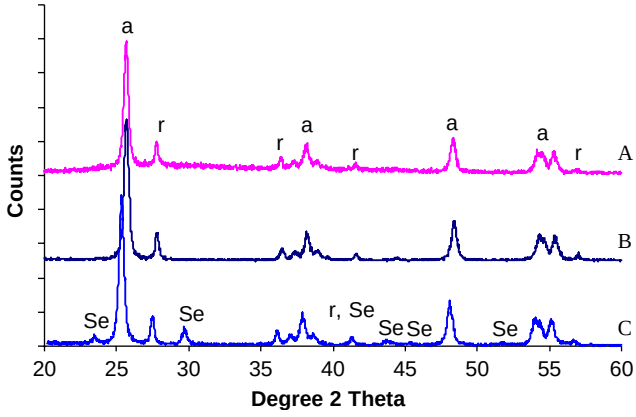

Fig. 10. XRD patterns of (A) pure P25; (B) wet Se-P25; (C) dried Se-P25. Note: The powder diffraction file cards were used for identification of anatase (a), rutile (r) and selenium phases (Powder Diffraction File, 1995).

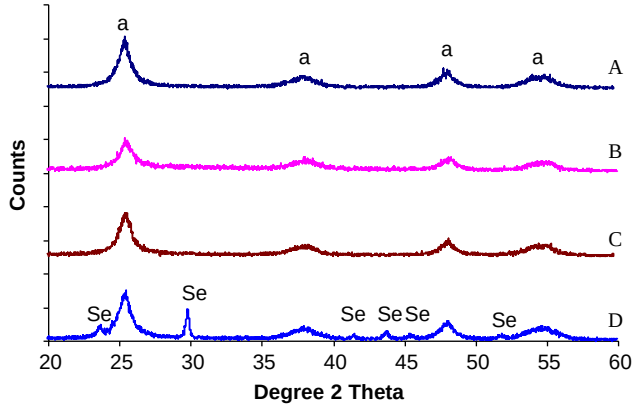

Fig. 11. XRD patterns of (A) pure PC500; (B) wet Se-PC500; (C) dried Se-PC500; (D) aged-dried Se-PC500. Note: The powder diffraction file cards were used for identification of anatase (a) and selenium phases (Powder Diffraction File, 1995).

reported that the metallic Se has the activation value ranging from 1.85 to 1.95 eV (Mort, 1968; Rajalakshmi and Arora, 1999; Tuthasi and Chen, 1967). Our values of 2.1 eV for amorphous Se and 1.82 eV for the stable form compared well with these values.

As was mentioned earlier, the Se-TiO_2 powders changed colour from orange-pink (wet Se-P25, wet PC50 and dried Se-PC500 powders) to purple (dried Se-P25) or grey (dried PC50 and aged-dried Se-PC500 powders). Hence, it is postulated that the Se deposits had undergone a transformation to a crystalline form during the drying and ageing process. This also suggests that the dried Se-P25 and Se-PC50 powders contained a large amount crystalline Se with a small admixture of amorphous phase while the dried Se-PC500 consisted of mostly amorphous Se and a small amount of the crystalline form.

The colour change of the Se-PC500 sample took a longer time to occur than for the Se-P25 and Se-PC50 samples. Quenching an amorphous Se colloid at room temperature, Gates et al. (2002) found the complete conversion of the amorphous form to the stable crystalline form of Se only after 10–20 days. A TGA analysis of the dried Se-P25 and dried Se-PC500 (not shown here) revealed that only 1% of the dried Se-P25 weight was lost when the temperature increased to 300 °C while the dried Se-P500 lost approximately 9% of its weight. It is therefore postulated that the delayed colour change of the Se-PC500 sample is due to its higher water content due to the porous structure of PC500 compared to P25 and PC50 which slowed down the transformation process of the amorphous Se(0) deposits to their crystalline form.

To verify the phase transformation of the Se(0) deposits, the wet and dried Se-P25 (Fig. 10) and the wet, dried and aged-dried Se-PC500 (Fig. 11) were subjected to XRD analysis. The XRD patterns for P25 and PC500 were also obtained.

First, it is noted that as P25 consists of anatase and rutile, the peaks characterised for both phases were observed in the XRD pattern (line A, Fig. 10) while the XRD pattern for PC500 showed only peaks for anatase, indicating that PC500 contains mainly anatase (line A, Fig. 11). It is also observed that the anatase peaks in the XRD spectrum for P25 is sharper than those in the PC500 XRD spectrum due to larger crystal size of TiO_2 in P25 compared to that in PC500.

As discussed earlier, the P25 and PC500 are white in colour while the wet Se-P25 and wet Se-PC500 powders had an orange-pink colour, indicating the presence of Se(0) deposits. As can be seen in Figs. 10 and 11, the XRD patterns obtained for the wet Se-P25 (line B, Fig. 10) and wet

Se-PC500 (line B, Fig. 11) resembled those of P25 (line A, Fig. 10) and PC500 (line A, Fig. 11), respectively. This suggests that the freshly deposited Se(0) was amorphous in nature, which could not be detected by XRD. When the wet orange-pink Se-P25 was dried in an oven at 60 °C, the colour of the powder changed to purple and its XRD pattern showed the presence of crystalline Se(0) (line C, Fig. 10). This confirms our postulation that when P25 was used the Se(0) deposits had undergone a phase transformation during the drying process. The dried Se-PC500 on the other hand, was still orange-pink coloured, and its XRD pattern (line C, Fig. 11) was similar to that of the wet Se-PC500 (line B, Fig. 11) suggesting that the Se(0) deposits were still in the amorphous phase. However, the XRD pattern obtained for the dried Se-PC500 after 2 weeks ageing revealed that the Se(0) deposits were crystallised (line D, Fig. 11). This, again confirms that the amorphous Se(0) on the dried Se-PC500 had transformed to the crystalline form during the ageing process. As amorphous selenium has various electrical and optical uses, due to its photoconducting properties (Kirk-Othmer, 1997), the delayed phase transformation of amorphous Se(0) observed in the PC500 system might be beneficial for some applications.

4. Conclusions

Under similar conditions, the performance of Millennium PC500 for adsorption and photoreduction of selenite and selenate was better than that of Degussa P25 and Millennium PC50. This was attributed to its higher surface area and greater adsorption of the selenium ions compared to that of P25 and PC50. P25 and PC50 with similar surface area exhibited comparable performance for the photoreduction of selenite and selenate. Furthermore, UV–Vis reflectance measurements and XRD characterisation revealed that during the drying and ageing process, the Se(0) deposits had undergone a transformation to their crystallite form, which extended their absorbance spectra from around 580 nm to a longer wavelength at 680 nm. From the current study, it can be concluded that the Millennium PCs are promising TiO_2-based photocatalysts for the photoreduction of selenium ions.

Acknowledgements

We thank the academic and technical staff from the School of Chemical Science, UNSW for their assistance with using the UV–Vis Cary 5 instrument, the School of Materials Science for their assistance with the use of XRD instrument, and the Electron Microscope Unit, UNSW, for their assistance with the use of TEM. Vi N. H. Nguyen acknowledges AusAID for the scholarship provided for her Ph.D. study. This work was produced as part of the activities of the ARC Centre for Functional Nanomaterials funded by the Australian Research Council under the ARC Centres of Excellence Program.

References

Al-Ani, S.K.J., Al-Delaimi, M.N., Munaim, A.H.A., Jawher, H.M., 1990. Optical and electrical properties of pure and doped amorphous thin selenium films. International Journal of Electronics 69 (1), 87–95.

Almquist, A.B., Biswas, P., 2002. Role of synthesis method and particle size of nanostructured TiO_2 on its photoactivity. Journal of Catalysis 212, 145–156.

Arabatzis, I.M., Antonaraki, S., Stergiopoulos, T., Hiskia, A., Papaconstantinou, E., Bernard, M.C., Falaras, P., 2002. Preparation, characterisation and photocatalytic activity of nanocrystalline thin film TiO_2 catalysts toward 3,5-dichlorophenol degradation. Journal of Photochemistry and Photobiology A: Chemistry 149, 237–245.

Arslan, I., Balcioglu, I.A., Bahnemann, D.W., 2000. Heterogeneous photocatalytic treatment of simulated dyehouse effluents using novel TiO_2-photocatalysts. Applied Catalysis B: Environmental 26, 193–206.

Calvert, J.G., Pitts Jr., J.N., 1966. Chapter 7: Experimental methods in photochemistry. In: Photochemistry.Wiley, New York, pp. 686–814.

Campostrini, R., Carturan, G., Palmisano, L., Schiavello, M., Sclafani, A., 1994. Sol-gel derived anatase TiO_2: morphology and photoactivity. Materials Chemistry and Physics 38, 277–283.

Chen, D., Ray, A.K., 2001. Removal of toxic metal ions form wastewater by semiconductor photocatalysis. Chemical Engineering Science 56, 1561–1570.

Colon, G., Hidalgo, M.C., Navio, J.A., 2001. Photocatalytic deactivation of commercial TiO_2 samples simultaneous photoreduction of Cr(VI) and photooxidation of salicylic acid. Journal of Photochemistry and Photobiology A: Chemistry 138, 79–85.

Cotton, A.F., Wilkinson, G., 1988. Advanced Inorganic Chemistry. fifth ed. A Wiley-Interscience Publication, Wiley, New York, Chichester, Brisbane, Toronto, Singapore.

Delgass, W.N., Haller, G.L., Kellerman, R., Lunsford, J.H., 1979. Chapter 4: Diffuse reflectance and photoacoustic spectroscopies. In: Spectroscopy in Heterogeneous Catalysis.Academic Press, New York, San Francisco, London, pp. 86–129.

Gates, B., Mayers, B., Cattle, B., Xia, Y., 2002. Synthesis and characterization of uniform nanowires of trigonal selenium. Advanced Functional Materials 12 (3), 219–227.

Greenwood, N.N., Earnshaw, A., 1997. Chemistry of the Elements. second ed. Butterworth and Heinemann, Stoneham, MA.

Guillard, C., Lachheb, H., Houas, A., Ksibi, M., Elaloui, E., Herrmann, J.M., 2003. Influence of chemical structure of dyes, of pH and of inorganic salts on their photocatalytic degradation by TiO_2 comparison of the efficiency of powder and supported TiO_2. Journal of Photochemistry and Photobiology A: Chemistry 158, 27–36.

Hatchard, C.G., Parker, C.A., 1956. A new sensitive chemical actinometer. II. Potassium ferrioxalate as a standard chemical actinometer. Proceedings of Royal Society of London A 325, 518–536.

Herrmann, J.M., Guillard, C., Disdier, J., Lehaut, C., Malato, S., Blanco, J., 2002. New industrial titania photocatalysts for the solar detoxification of water containing various pollutants. Applied Catalysis B: Environmental 35, 281–294.

Howe, R.F., 1998. Recent development in photocatalysis. Development of Chemical Engineering in Mineral Processes 61 (1/2), 55–84.

Hufschmidt, D., Bahnemann, D., Testa, J.J., Emilio, C.A., Litter, M.I., 2002. Enhancement of the photocatalytic activity of various TiO_2 materials by platinisation. Journal of Photochemistry and Photobiology A: Chemistry 148, 223–231.

Kirk-Othmer, 1997. Encyclopedia of Chemical Technology, fourth ed. vol. 21. A Wiley-Interscience Publication, New York, p. 686.

Lemly, A.D., 2004. Aquatic selenium pollution is a global environmental safety issue. Ecotoxicology and Environmental Safety 59 (1), 44–56.

Litter, M.I., 1999. Review: heterogeneous photocatalysis—transition metal ions in photocatalytic system. Applied Catalysis B: Environmental 23, 89–114.

Mandough, Z.S.E., 1993. Effect of ageing on some physical properties of selenium thin films. Fizika 2 (1), 35–42.

Mills, A., Le Hunte, S., 1997. An overview of semiconductor photocatalysis. Journal of Photochemistry and Photobiology A: Chemistry 108, 1–35.

Mort, J., 1968. Transient photoconductivity in trigonal selenium single crystals. Journal of Applied Physics 39 (8), 3543–3549.

Nguyen, N.H.V., Beydoun, D., Amal, R., 2004. Photocatalytic reduction of selenite and selenate using TiO_2 photocatalyst. Journal of Photochemistry and Photobiology A: Chemistry 171, 117–124.

Peled, A., Perakh, M., 1985. Electrical and photoelectric properties of photodeposited a-Se films. International Journal of Electronics 58 (3), 381–393.

Powder Diffraction File: Inorganic phases, International Centre for Diffraction Data, Pennsylvania, 1995.

Rajalakshmi, M., Arora, A.K., 1999. Optical properties of selenium nanoparticles dispersed in polymer. Solid State Communications 110, 75–80.

Sanuki, S., Kojima, T., Arai, K., Nagaoka, S., Majima, H., 1999. Photocatalytic reduction of selenate and selenite solutions using TiO_2 powders. Metallurgical and Materials Transaction B 30B, 15–20.

Sclafani, A., Herrmann, J.M., 1996. Comparison of the photoelectronic and photocatalytic activities of various anatase and rutile forms of titania in pure liquid organic phases and in aqueous solutions. Journal of Physical Chemistry 100, 13 655–13.

Sclafani, A., Palmisano, L., Schiavello, M., 1990a. Influence of the preparation methods of TiO_2 on the photocatalytic degradation of phenol in aqueous dispersion. Journal of Physical Chemistry 94, 829–832.

Sclafani, A., Palmisano, L., Davi, E., 1990b. Photocatalytic degradation of phenol by TiO_2 aqueous dispersions: rutile and anatase activity. New Journal of Chemistry 14, 265–268.

Seby, F., Potin-Gautier, M., Giffaut, E., Borge, G., Donard, O.F.X., 2001. A critical review of thermodynamic data for selenium species at 25 °C. Chemical Geology 171, 173–194.

Serpone, N., Borgarello, E., Pelizzetti, E., 1988. Photoreduction and photodegradation of inorganic pollutants: II. Selective reduction and recovery of Au, Pt, Pd, Rh, Hg and Pb. In: Schiavello, M. (Ed.), Photocatalysis and Environment, Trends and Applications. Kluwer Academic Publishers, Dordretch, Boston, London, pp. 527–565.

Sharmasarkar, S., Vance, G.F., 2002. Selenite–selenate sorption in surface coalmine environment. Advances in Environmental Research 7, 87–95.

Tahiri, H., Serpone, N., van Mao, R.L., 1996. Application of concept of relative photonic efficiencies and surface characterization of a new titania photocatalyst designed for environmental remediation. Journal of Photochemistry and Photobiology A: Chemistry 93, 199–203.

Tan, T.Y.T., Zaw, M., Beydoun, D., Amal, R., 2002. The formation of nano-sized dioxide composite semiconductors by photocatalysis. Journal of Nanoparticle Research 4, 541–552.

Tan, T.T.Y., Beydoun, D., Amal, R., 2003. Photocatalytic reduction of Se(VI) in aqueous solutions in UV/TiO_2 system: importance of optimum ratio of reactants on TiO_2 surface. Journal of Molecular Catalysis A: Chemistry 202, 73–85.

Theuric, J., Lindner, M., Bahnemann, D.W., 1996. Photocatalytic degradation of 4-chlorophenol in aerated aqueous titanium dioxide suspensions: a kinetic and mechanistic study. Langmuir 12, 6368–6376.

Tuthasi, S., Chen, I., 1967. Optical properties and band structure of trigonal selenium. Physical Review 158 (3), 623–630.

Wang, C., Rabani, J., Bahnemann, D.W., Dohrmann, J.K., 2002. Photonic efficiency and quantum yield of formaldehyde formation from methanol in the presence of various TiO_2 photocatalysts. Journal of Photochemistry and Photobiology A: Chemistry 148, 169–176.

Wang, X., Pehkonen, S.O., Ray, A.K., 2004. Photocatalytic reduction of Hg(II) on two commercial TiO_2 catalysts. Electrochimica Acta 49, 1435–1444.